Research Square

Preprints are preliminary reports that have not undergone peer review.
They should not be considered conclusive, used to inform clinical practice,
or referenced by the media as validated information.

WASP-193b: An extremely low-density super-Neptune

Khalid Barkaoui (khalid.barkaoui@uliege.be)
University of Liège

Francisco Pozuelos
University of Liège

Coel Hellier
Keele University

Barry Smalley
Keele University https://orcid.org/0000-0002-3456-087X

Louise D. Nielsen
Université de Genève

Caroline Dorn
University of Zurich https://orcid.org/0000-0001-6110-4610

Michaël Gillon
University of Liège https://orcid.org/0000-0003-1462-7739

Ravit Helled
University of Zurich https://orcid.org/0000-0001-5555-2652

Simon Müller
University of Zurich https://orcid.org/0000-0002-8278-8377

Emmanuel Jehin
Universite de Liege

Brice-Olivier Demory
University of Bern, Center for Space and Habitability, Gesellschaftsstrasse 6, CH-3012, Bern, Switzerland
https://orcid.org/0000-0002-9355-5165

Prajwal Niraula
MIT

Abderahmane Soubkiou
Cadi Ayyad University

Mourad Ghachoui
Cadi Ayyad University

David. R. Anderson
University of Warwick

Zouhair Benkhaldoun
Cadi Ayyad University

Francois Bouchy
Geneva University
Artem Burdanov
Julien de Wit
MIT https://orcid.org/0000-0003-2415-2191
Laetitia Delrez
Université de Liège https://orcid.org/0000-0001-6108-4808
Elsa Ducrot
Université de Paris
Lionel Garcia
University of Liège
Abdelhadi Jabiri
Cadi Ayyad University
Monika Lendl
Université de Genève
Pierre Maxted
Keele University
Catriona Murray
University of Cambridge
Peter Pedersen
University of Cambridge
Didier Queloz
Cambridge University https://orcid.org/0000-0002-3012-0316
Daniel Sebastian
University of Liege
Oliver Turner
Université de Genève
Stéphane Udry
University of Geneva https://orcid.org/0000-0001-7576-6236
Mathilde Timmermans
University of Liège
Amaury Triaud
University of Birmingham https://orcid.org/0000-0002-5510-8751
Richard West
University of Warwick https://orcid.org/0000-0001-6604-5533

Article

Keywords:

Posted Date: March 17th, 2022

DOI: https://doi.org/10.21203/rs.3.rs-1411313/v1

License: This work is licensed under a Creative Commons Attribution 4.0 International License.
Read Full License

WASP-193 b: An extremely low-density super-Neptune

Khalid Barkaoui[1,2] *, Francisco J. Pozuelos[1,3], Coel Hellier[4], Barry Smalley[4], Louise D. Nielsen[5,6], Caroline Dorn[7], Michaël Gillon[1], Ravit Helled[7], Simon Müller[7], Emmanuel Jehin[3], Brice-Olivier Demory[8], Prajwal Niraula[10], Abderahmane Soubkiou[2], Mourad Ghachoui[1,2], David. R. Anderson[9], Zouhair Benkhaldoun[2], Francois Bouchy[5], Artem Burdanov[10], Julien de Wit[10], Laetitia Delrez[1,3], Elsa Ducrot[11,12], Lionel Garcia[1], Abdelhadi Jabiri[2], Monika Lendl[5], Pierre F. L. Maxted[4], Catriona A. Murray[13], Peter Pihlmann Pedersen[13], Didier Queloz[5,13], Daniel Sebastian[14], Oliver Turner[5,16], Stephane Udry[5], Mathilde Timmermans[1], Amaury H. M. J. Triaud[14], and Richard G. West[9,15]

[1] *Astrobiology Research Unit, Université de Liège, 19C Allée du 6 Août, 4000 Liège, Belgium*
[2] *Oukaimeden Observatory, High Energy Physics and Astrophysics Laboratory, Faculty of sciences Semlalia, Cadi Ayyad University, Marrakech, Morocco*
[3] *Space sciences, Technologies and Astrophysics Research (STAR) Institute, Université de Liège, Belgium*
[4] *Astrophysics Group, Keele University, Staffordshire, ST5 5BG, UK*
[5] *Observatoire de Genève, Université de Genève, Chemin Pegasi 51, 1290 Sauverny, Switzerland*
[6] *European Southern Observatory, Karl-Schwarzschildstr. 2, D-85748 Garching bei München, Germany*
[7] *University of Zurich, Institute of Computational Sciences, Winterthurerstrasse 190, CH-8057 Zurich, Switzerland*
[8] *Center for Space and Habitability, University of Bern, Gesellschaftsstrasse 6, CH-3012, Bern, Switzerland*
[9] *Department of Physics, University of Warwick, Gibbet Hill Road, Coventry CV4 7AL, UK*
[10] *Department of Earth, Atmospheric and Planetary Science, Massachusetts Institute of Technology, 77 Massachusetts Avenue, Cambridge, MA 02139, USA*
[11] *Paris Region Fellow, Marie Sklodowska-Curie Action*
[12] *AIM, CEA, CNRS, Université Paris-Saclay, Université de Paris, F-91191 Gif-sur-Yvette, France*
[13] *Cavendish Laboratory, JJ Thomson Avenue, Cambridge, CB3 0H3, UK*
[14] *School of Physics & Astronomy, University of Birmingham, Edgbaston, Birmingham, B15 2TT, UK*
[15] *Centre for Exoplanets and Habitability, University of Warwick, Gibbet Hill Road, Coventry CV4 7AL, UK*
[16] *Space Forge, Unit 10, Eastgate Business Park, Wentloog Ave, Rumney, Cardiff, CF3 2EY*

Gas giants transiting bright nearby stars are key objects for our understanding of planetary system formation and evolution mechanisms. This paper presents a new transiting exoplanet discovered by the WASP-South transit survey, WASP-193 b. WASP-193 b orbits its $V_{\rm mag} = 12.0$ F9 main-sequence host star every 6.25 d. Our analyses found that WASP-193 b has a mass of $M_p = 0.146 \pm 0.033\ M_{\rm Jup}$, a radius of $R_P = 1.58 \pm 0.14\ R_{\rm Jup}$, translating into an extremely low density of $\rho_p = 0.049 \pm 0.015$ g cm^{-3}. The planet was confirmed photometrically by the 0.6-m TRAPPIST-South and 1.0-m SPECULOOS-South telescopes and spectroscopically by the ESO-3.6-m/HARPS and Euler-1.2-m/CORALIE spectrographs. The combination of its large transit depth ($dF \sim 1.4$ %), its super-low density, its high-equilibrium temperature ($T_{\rm eq} = 1275 \pm 40\ K$), and the infrared brightness of its host star (magnitude $K_{\rm mag} = 10.7$) makes WASP-193 b an exquisite target for a detailed atmospheric characterization by transmission spectroscopy.

The WASP (Wide Angle Search for Planets[1]) ground-based transit survey has discovered almost 200 planets, transiting bright nearby stars mostly, hot Jupiters plus some short-period Saturn- and

*corresponding author (khalid.barkaoui@uliege.be)

Neptune-mass objects. Many WASP planets have proven to be favorable targets for detailed atmospheric characterization with large ground-based telescopes (e.g. *VLT*[2], *E-ELT*[3], *Magellan*[4]), *HST*[5] and *JWST*[6], e.g. WASP-17 b[7]. The project consists of data obtained at telescopes located at two sites: Sutherland Station of the South African Astronomical Observatory (SAAO) and the Observatorio del Roque de Los Muchachos on La Palma in the Canary Islands. The field-of-view (FOV) of each instrument was 482 deg^2 with a pixel scale of 13.7" pixel^{-1}. These instruments were capable of obtaining photometry with a precision better than 1% for objects with V-magnitudes between 7.0 and 11.5[1]. The WASP-South and WASP-North data calibration (bias and dark subtraction, and flat-field division) was performed using a bespoke pipeline [8]. Aperture photometry was performed on the final calibrated images, where the star's fluxes were measured in three apertures with radii of 2.5, 3.5, and 4.5 pixels, following the method described by ref. [1,8,9].

WASP-193 was observed by the WASP-South survey in 2006–2008 and 2011–2012. The WASP photometry revealed a periodic signal consistent with transits of a giant planet with an orbital period of 6.25d. Ground-based photometric follow-up was obtained using the TRAPPIST-South[10,11] and SPECULOOS-South[12–14] telescopes, and spectroscopic measurements were obtained using CORALIE[15] and HARPS[16] spectrographs. Additional photometric measurements were obtained by *TESS*[17] with the 30-min cadence during sector-9 of its primary mission and with 10-min cadence during sector-36 of its extended mission. The reduced transit light curves of WASP-193 b obtained with WASP-South, TESS, TRAPPIST-South, and SPECULOOS-South are presented in Fig. 1, 2 and 3, respectively.

In addition, we used the Euler-1.2m/CORALIE and ESO-3.6m/HARPS spectrographs to observe WASP-193. We obtained 12 and 11 spectroscopic measurements with CORALIE and HARPS in 2015 and 2019, respectively. We used the cross-correlation technique in order to extract the radial velocity measurements as described by ref. [18] (see Methods). The reduced radial velocity curve is presented in Fig. 4.

All the follow-up data were consistent with the planetary origin of the transit signal identified by WASP. Notably, the high-precision follow-up light curves acquired in different filters showed no chromatic dependence of the transit depth, the radial velocities showed a periodic signal with a period of 6.25d and a phase consistent with the transit timings, and the bisector analysis of the HARPS and CORALIE spectra[19] did not reveal any dependence of the measured radial velocities with the bisector span (Fig. 5).

To constrain the stellar atmospheric parameters of WASP-193, we co-added HARPS and CORALIE spectra to produce a single stellar spectra with a high signal-to-noise ratio (SNR$\sim$75) and analyzed it as described in ref. [20]. This analysis enabled us to constrain the following parameters: the spectral type, the metallicity $[Fe/H]$, the effective temperature $T_{\rm eff}$, the surface gravity $\log g_\star$, and the rotational velocity $V \sin(i)$ (see Methods). The resulting values show that WASP-193 is an F9-type Sun-like star with $T_{\rm eff} = 6076 \pm 120$ K, $\log g_\star = 4.256 \pm 0.044$ dex, $[Fe/H] = -0.16 \pm 0.09$ dex

and $V \sin(i) = 4.3 \pm 0.8$ km s^{-1}. Using the *EXOFASTv2* pipeline and magnitudes of the star in different broadband filters (Table 1), we derived stellar parameters in good agreement with those derived from our spectroscopic analysis (Table 2). We used the inferred stellar atmospheric parameters and the stellar evolution modeling code BAGEMASS to derive an age of 4.95 ± 1.34 Gyr for the star (see Methods). Table 2 summarizes the stellar parameters inferred from our different spectroscopic analyses.

We performed a global analysis of the WASP and follow-up photometry, and radial velocity measurements to constrain the system's parameters, using the latest version of the Markov Chain Monte Carlo (MCMC) code described in ref. [21]. We modeled the photometric and spectroscopic data using the Mandel & Agol model [22] and a 2-body Keplerian model [23], respectively (see Methods). Table 3 shows the deduced stellar and planetary physical parameters and their 1–σ intervals.

We find that planet has a radius of 1.58 ± 0.14 $R_{\rm Jup}$ and a mass of 0.146 ± 0.033 $M_{\rm Jup}$ ($\sim$ 3 $M_{\rm Neptune}$), resulting in a surprisingly low density of 0.049 ± 0.015g cm^{-3} (see Fig. 6 and 7). Considering the irradiation of 6×10^5 W/m^2 inferred for the planet (see Fig. 8), classical evolution models of irradiated giant planets[24–27] are not able to reproduce WASP-193b's radius. The planet joins thus the sub-group of 'anomalously large' irradiated gas giants[28].

Planet Interior

In the core accretion model, planets at this mass range are expected to be heavy-element dominated. This is at odds with the low density of WASP-193 b. Alternatively, the planet could have formed by disk instability, as it was recently shown by ref. [29] that magnetically controlled disk fragmentation could lead to intermediate-mass clumps of H-He. The formation mechanism of planets like WASP-193 b remains uncertain, including its potential orbital evolution and we hope that future formation models can address its formation mechanism. The composition of the planet is also puzzling. A model that accounts for stellar irradiation and residual heat from formation can lead to large radii for the mass of WASP-193 b by assuming a composition that is dominated by H-He. However, these radii shrink significantly below the observed radius after Gyr-timescales. Fig. 9 (solid line) shows the radius evolution of an (unrealistic) bulk composition of pure H-He (i.e., $Z = 0.0$; with a helium mass fraction of 0.275).

For the evolution model we use the model presented by ref.[30], using the equations of state[31] for He-He and for a water-rock mix[32]. The planetary radius corresponds to the photosphere where the optical depths drop below 2/3. Gas opacities are taken from ref.[33]. Additional details on the interior evolution model can be found in ref.[30]. No stellar evolution is considered in the model, but we tested that the consideration of the early evolution of the host star only marginally affects the calculated evolution curves.

Even for the extreme case of pure H-He interior, the radius drops below 1.1 $R_{\rm Jup}$ after a few Gyrs.

It was shown by ref. [34] that interiors with moderate metallicities can results in slower cooling due to enhanced atmospheric opacities, and therefore slower contraction. We therefore also consider a model with 10 % heavy elements (Z = 0.1, specifically, 5 % H_2O and 5% SiO_2). Although in this case the radius is ∼10 % larger than the pure H-He composition it still cannot reproduce the measured radius of WASP-193 b.

We estimate the additional amount of heating that is needed to explain the radius of WASP-193 b to be 10^{46} erg = 10^{39} Joule. This value is inferred by integrating the luminosity from the evolution model (Z = 0.1, Fig. 9) from a few Gyrs back to when the radius of 1.5 $R_{\rm Jup}$ was reached. We note that the required amount of energy from Ohmic dissipation can be different as it is deposited in the upper envelope instead of being equally deposited within the planet. Clearly, the large observed radius of 1.5 $R_{\rm Jup}$ at an age of several Gyr cannot be reproduced unless other mechanisms are at work, these include processes that (1) delay the cooling of the planet, or (2) deposit heat deep in the planetary interior. We discuss such mechanisms in detail below.

Delay in planetary cooling Inefficient cooling can be caused by various processes such as an enhanced atmospheric opacity that leads to longer cooling time scales, interiors that are not fully convective, and phase separations. For the former, as we show in Fig. 9; the effect of prolonged cooling via opacity enhancement is insufficient to explain WASP-193 b's large radius. Also in the case of a not fully convective interior, the planet contracts at a lower rate. This can occur when the interior consists of boundary layers and/or composition gradients [35–37]. Such a configuration can lead to much higher internal temperatures at a given age [38] and is expected to lead to an increase in radius by ∼10% [39]. Therefore, also this scenario cannot explain the large observed radius. Phase separation could also lead to slower cooling. In giant planets He-rain can delay the planetary cooling [40]. Its ability to increase the planetary radii is however limited to few percents [41]. More importantly, a planet of 0.15 $M_{\rm Jup}$ as WASP-193 b is not expected to reach internal pressures that are high enough for He to become immiscible [41].

A self-consistent model that incorporates layered-convection, boundary layers as well as enhanced opacities and dust-rich atmospheres to delay the cooling to its maximum would be required to evaluate whether the combined mechanisms are sufficient to explain the measured radius.

Heat deposition and mass loss The planet could be efficiently heated at depth, either driven by Ohmic dissipation, tidal heating, or stellar flux deposition at high pressures. Ohmic dissipation seems to be the most promising mechanism[42]. This is because the atmosphere of WASP-193 b is hot enough (with T_{eq} of 1275 K) that trace elements in the H-He gas can be partially ionized and allow for atmospheric currents to penetrate deep into the interior.

For hot Jupiters, the radius inflation power depends on incident flux[43]. If WASP-193 b experiences

similar inflation mechanisms, this suggests that mechanisms that are coupled to stellar heating, including Ohmic dissipation, are favorable and possibly, multiple mechanisms are at play.

Finally, the relatively low mass of WASP-193 b, its high stellar irradiation and its location at the edge of the sub-Jovian valley in the M-R diagram might hint that it is losing mass. If this is indeed the case, it is possible that the extended observed radius is related to material that is evaporating and leaving the planet. However, this is only a speculation, and we stress that there is no indication in the measurements for atmospheric loss.

Atmospheric characterization prospects

WASP-193 b has transmission spectroscopy metric (TSM [44]) of 607. The combination of the brightness of the parent star, super-low density of the planet, high equilibrium temperature, large amplitude of the transmission spectroscopy, large atmospheric scale-height ($H = 3008 \pm 119$ km) and high transmission spectroscopy metric, makes WASP-193 b an ideal target for atmospheric exploration using transmission spectroscopy with HST and JWST (see Fig. 11). Fig 12 shows a sample synthetic transmission spectrum for high metallicity atmosphere (mixing ratio: 10^{-3}) for WASP-193 b using JWST with a single transit observation in different grism modes with noise modeled using *pandexo*. Owing to its favorable TSM, thanks largely to the low gravity and large radius, the presence of major absorbers in the atmospheres from water, methane to carbon dioxide are easily detectable with a single transit observation with JWST in their respective bands. Similarly, a secondary eclipse depth (0.52mmag at $5\mu m$, 1.38mmag at $7.5\mu m$) can constrain properties of the dayside to provide chemical constraint on the atmosphere. Such observations will open our understanding on the nature of the inflated radius i.e. if the presence of high altitude clouds or hazes leads to an inflated radius of the planet. Similarly, constraining the temperature structure of the atmosphere, will help us understand how the the ultra-low density of WASP-193 hydrodynamically maintains its atmosphere despite the high stellar irradiation.

References

1. Pollacco, D. L. *et al.* The WASP project and the SuperWASP cameras. *Publications of the Astronomical Society of the Pacific* **118**, 1407–1418 (2006). URL https://doi.org/10.1086/508556.

2. Pepe, F. A. *et al.* ESPRESSO: the Echelle spectrograph for rocky exoplanets and stable spectroscopic observations. In McLean, I. S., Ramsay, S. K. & Takami, H. (eds.) *Ground-based and Airborne Instrumentation for Astronomy III*, vol. 7735, 209 – 217. International Society for Optics and Photonics (SPIE, 2010). URL https://doi.org/10.1117/12.857122.

3. Gilmozzi, R. & Spyromilio, J. The European Extremely Large Telescope (E-ELT). *The Messenger* **127**, 11 (2007).

4. Dressler, A. *et al.* IMACS: The inamori-magellan areal camera and spectrograph on magellan-baade. *Publications of the Astronomical Society of the Pacific* **123**, 288–332 (2011). URL https://doi.org/10.1086/658908.

5. Meylan, G., Madrid, J. P. & Macchetto, D. Hubble Space Telescope Science Metrics. *Publ. Astron. Soc. Pacific* **116**, 790–796 (2004). astro-ph/0406655.

6. Gardner, J. P. *et al.* The James Webb Space Telescope. *Space Science Reviews* **123**, 485–606 (2006). astro-ph/0606175.

7. Sing, D. K. *et al.* A continuum from clear to cloudy hot-Jupiter exoplanets without primordial water depletion. *Nature* **529**, 59–62 (2016). 1512.04341.

8. Collier Cameron, A. *et al.* A fast hybrid algorithm for exoplanetary transit searches. *Mon. Not. R. Astron. Soc.* **373**, 799–810 (2006). astro-ph/0609418.

9. Street, R. A. *et al.* Status of SuperWASP I (La Palma). *Astronomische Nachrichten* **325**, 565–567 (2004).

10. Gillon, M. *et al.* TRAPPIST: a robotic telescope dedicated to the study of planetary systems. *EPJ Web of Conferences* **11**, 06002 (2011). URL https://doi.org/10.1051/epjconf/20101106002.

11. Jehin, E. *et al.* TRAPPIST: TRAnsiting Planets and PlanetesImals Small Telescope. *The Messenger* **145**, 2–6 (2011).

12. Burdanov, A., Delrez, L., Gillon, M. & Jehin, E. SPECULOOS exoplanet search and its prototype on TRAPPIST. *ArXiv e-prints* (2017). 1710.03775.

13. Delrez, L. *et al.* SPECULOOS: a network of robotic telescopes to hunt for terrestrial planets around the nearest ultracool dwarfs. *ArXiv e-prints* (2018). 1806.11205.

14. Jehin, E. *et al.* The SPECULOOS Southern Observatory Begins its Hunt for Rocky Planets. *The Messenger* **174**, 2–7 (2018).

15. Queloz, D. *et al.* Extrasolar Planets in the Southern Hemisphere: The CORALIE Survey. In Bergeron, J. & Renzini, A. (eds.) *From Extrasolar Planets to Cosmology: The VLT Opening Symposium*, 548 (2000).

16. Mayor, M. *et al.* Setting New Standards with HARPS. *The Messenger* **114**, 20–24 (2003).

17. Ricker, G. R. *et al.* Transiting Exoplanet Survey Satellite (TESS). *Journal of Astronomical Telescopes, Instruments, and Systems* **1**, 014003 (2015).

18. Baranne, A. *et al.* ELODIE: A spectrograph for accurate radial velocity measurements. *Astron. Astrophys., Suppl. Ser.* **119**, 373–390 (1996).

19. Torres, G., Konacki, M., Sasselov, D. D. & Jha, S. Testing blend scenarios for extrasolar transiting planet candidates. i. OGLE-TR-33: A false positive. *The Astrophysical Journal* **614**, 979–989 (2004). URL https://doi.org/10.1086/423734.

20. Doyle, A. P. *et al.* Accurate spectroscopic parameters of WASP planet host stars. *Mon. Not. R. Astron. Soc.* **428**, 3164–3172 (2013). 1210.5931.

21. Gillon, M. *et al.* The TRAPPIST survey of southern transiting planets. I. Thirty eclipses of the ultra-short period planet WASP-43 b. *Astron. Astrophys.* **542**, A4 (2012). 1201.2789.

22. Mandel, K. & Agol, E. Analytic Light Curves for Planetary Transit Searches. *Astrophys. J., Letters* **580**, L171–L175 (2002). astro-ph/0210099.

23. Murray, C. D. & Correia, A. C. M. *Keplerian Orbits and Dynamics of Exoplanets*, 15–23 (2010).

24. Fortney, J. J., Marley, M. S. & Barnes, J. W. Planetary Radii across Five Orders of Magnitude in Mass and Stellar Insolation: Application to Transits. *Astrophys. J.* **659**, 1661–1672 (2007). astro-ph/0612671.

25. Baraffe, I., Chabrier, G. & Barman, T. Structure and evolution of super-Earth to super-Jupiter exoplanets. I. Heavy element enrichment in the interior. *Astron. Astrophys.* **482**, 315–332 (2008). 0802.1810.

26. Weiss, L. M. *et al.* The Mass of KOI-94d and a Relation for Planet Radius, Mass, and Incident Flux. *Astrophys. J.* **768**, 14 (2013). 1303.2150.

27. Sestovic, M., Demory, B.-O. & Queloz, D. Investigating hot-Jupiter inflated radii with hierarchical Bayesian modelling. *Astronomy & Astrophysics* **616**, A76 (2018). 1804.03075.

28. Lopez, E. D. & Fortney, J. J. RE-INFLATED WARM JUPITERS AROUND RED GIANTS. *The Astrophysical Journal* **818**, 4 (2016). URL https://doi.org/10.3847/0004-637x/818/1/4.

29. Deng, H., Mayer, L. & Helled, R. Formation of intermediate-mass planets via magnetically controlled disk fragmentation. *Nature Astronomy* **5**, 440–444 (2021).

30. Müller, S. & Helled, R. Synthetic evolution tracks of giant planets. *Monthly Notices of the Royal Astronomical Society* **507**, 2094–2102 (2021).

31. Chabrier, G., Mazevet, S. & Soubiran, F. A new equation of state for dense hydrogen–helium mixtures. *The Astrophysical Journal* **872**, 51 (2019).

32. More, R., Warren, K., Young, D. & Zimmerman, G. A new quotidian equation of state (qeos) for hot dense matter. *The Physics of fluids* **31**, 3059–3078 (1988).

33. Freedman, R. S. *et al.* Gaseous mean opacities for giant planet and ultracool dwarf atmospheres over a range of metallicities and temperatures. *The Astrophysical Journal Supplement Series* **214**, 25 (2014).

34. Müller, S., Helled, R. & Cumming, A. The challenge of forming a fuzzy core in jupiter. *Astronomy & Astrophysics* **638**, A121 (2020).

35. Chabrier, G. & Baraffe, I. Heat transport in giant (exo) planets: a new perspective. *The Astrophysical Journal Letters* **661**, L81 (2007).

36. Helled, R. & Stevenson, D. The fuzziness of giant planets' cores. *The Astrophysical Journal Letters* **840**, L4 (2017).

37. Vazan, A., Helled, R. & Guillot, T. Jupiter's evolution with primordial composition gradients. *Astronomy & Astrophysics* **610**, L14 (2018).

38. Leconte, J. & Chabrier, G. A new vision of giant planet interiors: Impact of double diffusive convection. *Astronomy & Astrophysics* **540**, A20 (2012).

39. Kurokawa, H. & Inutsuka, S.-i. On the radius anomaly of hot jupiters: Reexamination of the possibility and impact of layered convection. *The Astrophysical Journal* **815**, 78 (2015).

40. Stevenson, D. & Salpeter, E. The dynamics and helium distribution in hydrogen-helium fluid planets. *Astrophysical Journal Supplement Series* **35**, 239–261 (1977).

41. Fortney, J. J. & Hubbard, W. Effects of helium phase separation on the evolution of extrasolar giant planets. *The Astrophysical Journal* **608**, 1039 (2004).

42. Fortney, J. J., Dawson, R. I. & Komacek, T. D. Hot jupiters: Origins, structure, atmospheres. *Journal of Geophysical Research: Planets* **126**, e2020JE006629 (2021).

43. Thorngren, D. P. & Fortney, J. J. Bayesian Analysis of Hot-Jupiter Radius Anomalies: Evidence for Ohmic Dissipation? *Astron. J.* **155**, 214 (2018). 1709.04539.

44. Kempton, E. M. R. *et al.* A Framework for Prioritizing the TESS Planetary Candidates Most Amenable to Atmospheric Characterization. *Publications of the Astronomical Society of the Pacific* **130**, 114401 (2018). 1805.03671.

45. Hippke, M., David, T. J., Mulders, G. D. & Heller, R. Wōtan: Comprehensive Time-series Detrending in Python. *Astron. J.* **158**, 143 (2019). 1906.00966.

46. Masuda, K. Very Low Density Planets around Kepler-51 Revealed with Transit Timing Variations and an Anomaly Similar to a Planet-Planet Eclipse Event. *Astrophys. J.* **783**, 53 (2014). 1401.2885.

47. Zhou, G. *et al.* HAT-P-67b: An Extremely Low Density Saturn Transiting an F-subgiant Confirmed via Doppler Tomography. *Astron. J.* **153**, 211 (2017). 1702.00106.

48. Demory, B.-O. & Seager, S. Lack of Inflated radii for Kepler giant planet candidates receiving modest stellar irradiation. *The Astrophysical Journal Supplement Series* **197**, 12 (2011). URL https://doi.org/10.1088%2F0067-0049%2F197%2F1%2F12.

49. Mollière, P. *et al.* petitRADTRANS. A Python radiative transfer package for exoplanet characterization and retrieval. *Astron. Astrophys.* **627**, A67 (2019). 1904.11504.

50. Chambers, K. C. *et al.* The Pan-STARRS1 Surveys. *arXiv e-prints* arXiv:1612.05560 (2016). 1612.05560.

51. Gaia Collaboration *et al.* Gaia Data Release 2. Summary of the contents and survey properties. *Astron. Astrophys.* **616**, A1 (2018). 1804.09365.

52. Cutri, R. M. *et al. 2MASS All Sky Catalog of point sources.* (2003).

53. Henden, A. A. *et al.* VizieR Online Data Catalog: AAVSO Photometric All Sky Survey (APASS) DR9 (Henden+, 2016). *VizieR Online Data Catalog* II/336 (2016).

54. Wright, E. L. *et al.* The Wide-field Infrared Survey Explorer (WISE): Mission Description and Initial On-orbit Performance. *Astron. J.* **140**, 1868–1881 (2010). 1008.0031.

55. Doyle, A. P., Davies, G. R., Smalley, B., Chaplin, W. J. & Elsworth, Y. Determining stellar macroturbulence using asteroseismic rotational velocities from Kepler. *Monthly Notices of the Royal Astronomical Society* **444**, 3592–3602 (2014). URL https://doi.org/10.1093/mnras/stu1692. https://academic.oup.com/mnras/article-pdf/444/4/3592/6344008/stu1692.pdf.

56. Gray, R. O. & Corbally, C. J. An Expert Computer Program for Classifying Stars on the MK Spectral Classification System. *Astron. J.* **147**, 80 (2014).

57. Eastman, J. D. *et al.* EXOFASTv2: A public, generalized, publication-quality exoplanet modeling code. *arXiv e-prints* arXiv:1907.09480 (2019). 1907.09480.

58. Maxted, P. F. L., Serenelli, A. M. & Southworth, J. Bayesian mass and age estimates for transiting exoplanet host stars. *Astron. Astrophys.* **575**, A36 (2015). 1412.7891.

59. Barkaoui, K. *et al.* Discovery of Three New Transiting Hot Jupiters: WASP-161 b, WASP-163 b, and WASP-170 b. *Astron. J.* **157**, 43 (2019). 1807.06548.

60. Garcia, L. J. *et al.* prose: A Python framework for modular astronomical images processing. *Mon. Not. R. Astron. Soc.* (2021). 2111.02814.

61. Demory, B. O. *et al.* A super-Earth and a sub-Neptune orbiting the bright, quiet M3 dwarf TOI-1266. *Astron. Astrophys.* **642**, A49 (2020). 2009.04317.

62. Huang, C. X. *et al.* TESS Spots a Hot Jupiter with an Inner Transiting Neptune. *Astrophys. J., Letters* **892**, L7 (2020). 2003.10852.

63. Dong, J. *et al.* Warm Jupiters in TESS Full-frame Images: A Catalog and Observed Eccentricity Distribution for Year 1. *Astrophys. J., Suppl. Ser.* **255**, 6 (2021). 2104.01970.

64. Jenkins, J. M. *et al.* *The TESS science processing operations center*, vol. 9913 of *Society of Photo-Optical Instrumentation Engineers (SPIE) Conference Series*, 99133E (2016).

65. Zechmeister, M. & Kürster, M. The generalised Lomb-Scargle periodogram. A new formalism for the floating-mean and Keplerian periodograms. *Astron. Astrophys.* **496**, 577–584 (2009). 0901.2573.

66. Bruntt, H. *et al.* Accurate fundamental parameters for 23 bright solar-type stars. *Monthly Notices of the Royal Astronomical Society* **405**, 1907–1923 (2010). URL https://doi.org/10.1111/j.1365-2966.2010.16575.x. https://academic.oup.com/mnras/article-pdf/405/3/1907/17324571/mnras0405-1907.pdf.

67. Eastman, J., Gaudi, B. S. & Agol, E. EXOFAST: A Fast Exoplanetary Fitting Suite in IDL. *Publ. Astron. Soc. Pacific* **125**, 83 (2013). 1206.5798.

68. Gelman, A. & Rubin, D. B. Inference from Iterative Simulation Using Multiple Sequences. *Statistical Science* **7**, 457–472 (1992).

69. Gelman, A., Carlin, J. B., Stern, H. S. & Rubin, D. B. *Bayesian Data Analysis* (London: Chapman & Hall, 2003), 2 edn.

70. Choi, J. *et al.* Mesa Isochrones and Stellar Tracks (MIST). I. Solar-scaled Models. *Astrophys. J.* **823**, 102 (2016). 1604.08592.

71. Dotter, A. MESA Isochrones and Stellar Tracks (MIST) 0: Methods for the Construction of Stellar Isochrones. *Astrophys. J., Suppl. Ser.* **222**, 8 (2016). 1601.05144.

72. Gaia Collaboration *et al.* Gaia Data Release 1. Summary of the astrometric, photometric, and survey properties. *Astron. Astrophys.* **595**, A2 (2016). 1609.04172.

73. Stassun, K. G. & Torres, G. Evidence for a Systematic Offset of -80 μas in the Gaia DR2 Parallaxes. *Astrophys. J.* **862**, 61 (2018). 1805.03526.

74. Schlafly, E. F. & Finkbeiner, D. P. Measuring Reddening with Sloan Digital Sky Survey Stellar Spectra and Recalibrating SFD. *Astrophys. J.* **737**, 103 (2011). 1012.4804.

75. Weiss, A. & Schlattl, H. GARSTEC—the Garching Stellar Evolution Code. The direct descendant of the legendary Kippenhahn code. *Astrophysics and Space Science* **316**, 99–106 (2008).

76. Cassisi, S., Salaris, M. & Irwin, A. W. The Initial Helium Content of Galactic Globular Cluster Stars from the R-Parameter: Comparison with the Cosmic Microwave Background Constraint. *Astrophys. J.* **588**, 862–870 (2003). astro-ph/0301378.

77. Schwarz, G. Estimating the dimension of a model. *Ann. Statist.* **6**, 461–464 (1978). URL https://doi.org/10.1214/aos/1176344136.

78. Claret, A. & Bloemen, S. Gravity and limb-darkening coefficients for the Kepler, CoRoT, Spitzer, uvby, UBVRIJHK, and Sloan photometric systems. *Astron. Astrophys.* **529**, A75 (2011).

79. Hunter, J. D. Matplotlib: A 2d graphics environment. *Computing in Science Engineering* **9**, 90–95 (2007).

80. van der Walt, S., Colbert, S. C. & Varoquaux, G. The NumPy Array: A Structure for Efficient Numerical Computation. *Computing in Science and Engineering* **13**, 22–30 (2011). 1102.1523.

81. Astropy Collaboration *et al.* Astropy: A community Python package for astronomy. *Astron. Astrophys.* **558**, A33 (2013). 1307.6212.

82. Jones, E., Oliphant, T. & Peterson, P. SciPy: open source scientific tools for Python (2001). URL http://www.scipy.org.

83. Lightkurve Collaboration *et al.* Lightkurve: Kepler and TESS time series analysis in Python. Astrophysics Source Code Library (2018). 1812.013.

84. Hippke, M., David, T. J., Mulders, G. D. & Heller, R. Wōtan: Comprehensive Time-series Detrending in Python. *Astron. J.* **158**, 143 (2019). 1906.00966.

85. Bradley, L. *et al.* astropy/photutils: 1.0.0 (2020). URL https://doi.org/10.5281/zenodo.4044744.

Acknowledgments WASP-South is hosted by the South African Astronomical Observatory and we are grateful for their ongoing support and assistance. Funding for WASP comes from consortium universities and from the UK's Science and Technology Facilities Council. The research leading to these results has received funding from the European Research Council (ERC) under the FP/2007–2013 ERC grant agreement no. 336480, and under the H2020 ERC grant agreement no. 679030; and from an Actions de Recherche Concertée (ARC) grant, financed by the Wallonia-Brussels Federation. The Euler Swiss telescope by the Swiss National Science Foundation (SNF). This work has been carried out in part within the framework of the NCCR PlanetS supported by the Swiss National Science Foundation. This study is based on observations collected at the European Southern Observatory under ESO programme 0102.C-0414, PI: Nielsen. TRAPPIST-South is funded by the Belgian Fund for Scientific Research (Fond National de la Recherche Scientifique, FNRS) under the grant FRFC 2.5.594.09.F, with the participation of the Swiss National Science Fundation (SNF). M.G. and E.J. are FNRS Senior Research Associates. The ULiege's contribution to SPECULOOS has received funding from the European Research Council under the European Union's Seventh Framework Programme (FP/2007-2013) (grant Agreement n° 336480/SPECULOOS), from the Balzan Prize Foundation, from the Belgian Scientific Research Foundation (F.R.S.-FNRS; grant n° T.0109.20), from the University of Liege, and from the ARC grant for Concerted Research Actions financed by the Wallonia-Brussels Federation. This work is supported by a grant from the Simons Foundation (PI Queloz, grant number 327127). J.d.W. and MIT gratefully acknowledge financial support from the Heising-Simons Foundation, Dr. and Mrs. Colin Masson and Dr. Peter A. Gilman for Artemis, the first telescope of the SPECULOOS network situated in Tenerife, Spain. This work is supported by the Swiss National Science Foundation (PP00P2-163967, PP00P2-190080 and the National Centre for Competence in Research PlanetS). This work has received fund from the European Research Council (ERC) under the European Union's Horizon 2020 research and innovation programme (grant agreement n° 803193/BEBOP), from the MERAC foundation, and from the Science and Technology Facilities Council (STFC; grant n° ST/S00193X/1). C.D. was supported by the Swiss National Science Foundation (SNSF) under grant PZ00P2_174028. M.L. acknowledges support of the Swiss National Science Foundation under grant number PCEFP2_194576. E. D acknowledges support from the innovation and research Horizon 2020 program in the context of the Marie Sklodowska-Curie subvention 945298.

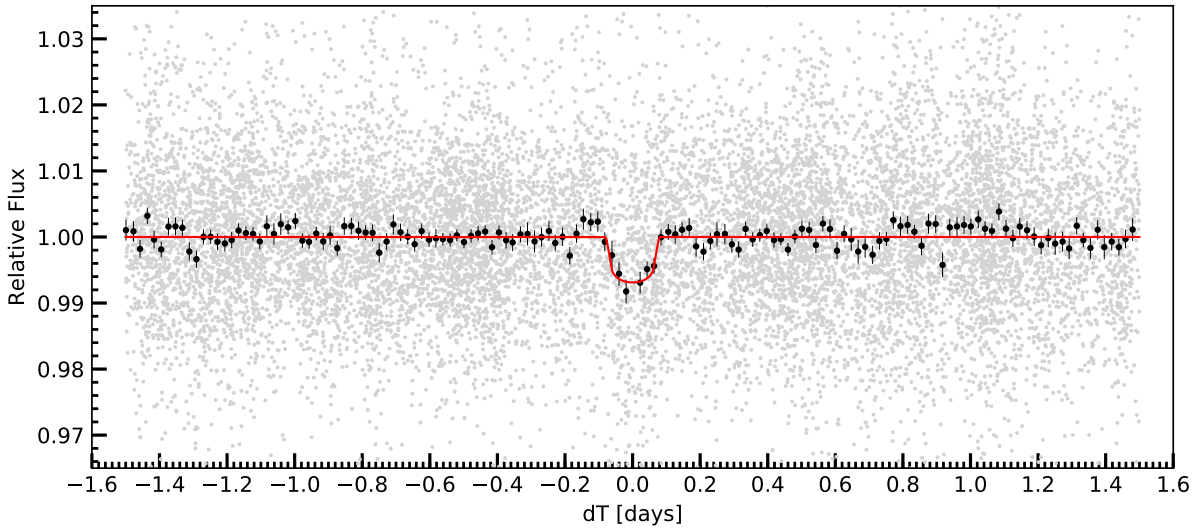

Figure 1: Detrended discovery light-curve of WASP-193 obtained with WASP-South (gray points: unbinned and black points: bin width = 30 min), period-folded using the orbital period deduced from our data analysis.

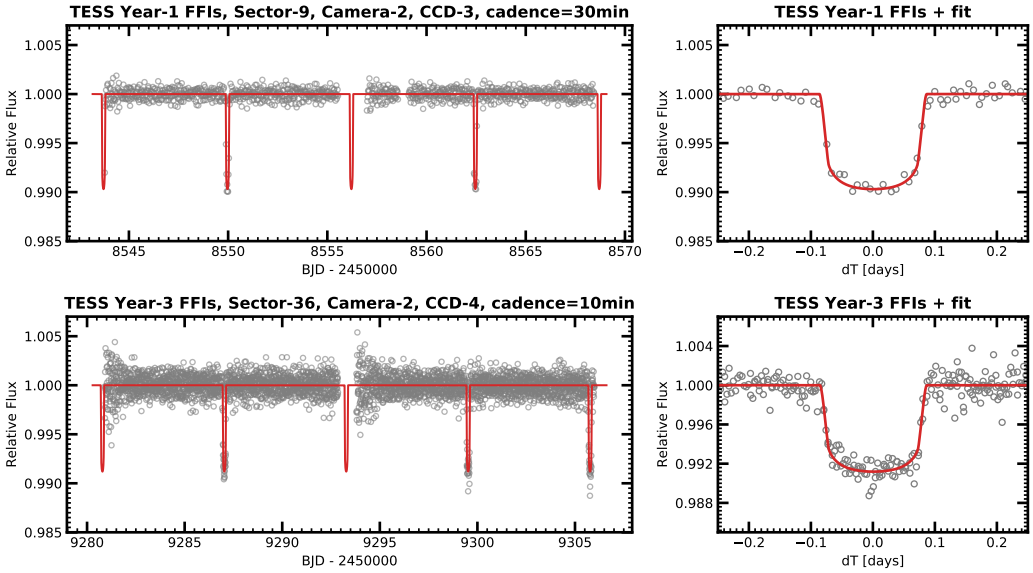

Figure 2: *TESS* light curves for WASP-193 taken in Sector-9 by CCD-3 of camera-2 with the 30-min cadence (from 28 February to 16 March 2019), and Sector-36 by CCD-4 of camera-2 with 10-min cadence (from 07 March to 02 April 2021). *Left panels:* Detrended *TESS* light curves obtained with the WOTAN package [45] using bi-weight method, in order to remove the instrumental systematic and stellar noise. *Right panels: TESS* light curve period-folded using the best-fitting transit ephemeris deduced from our global MCMC analysis. The red line is the best-fitting model superimposed on the light curve.

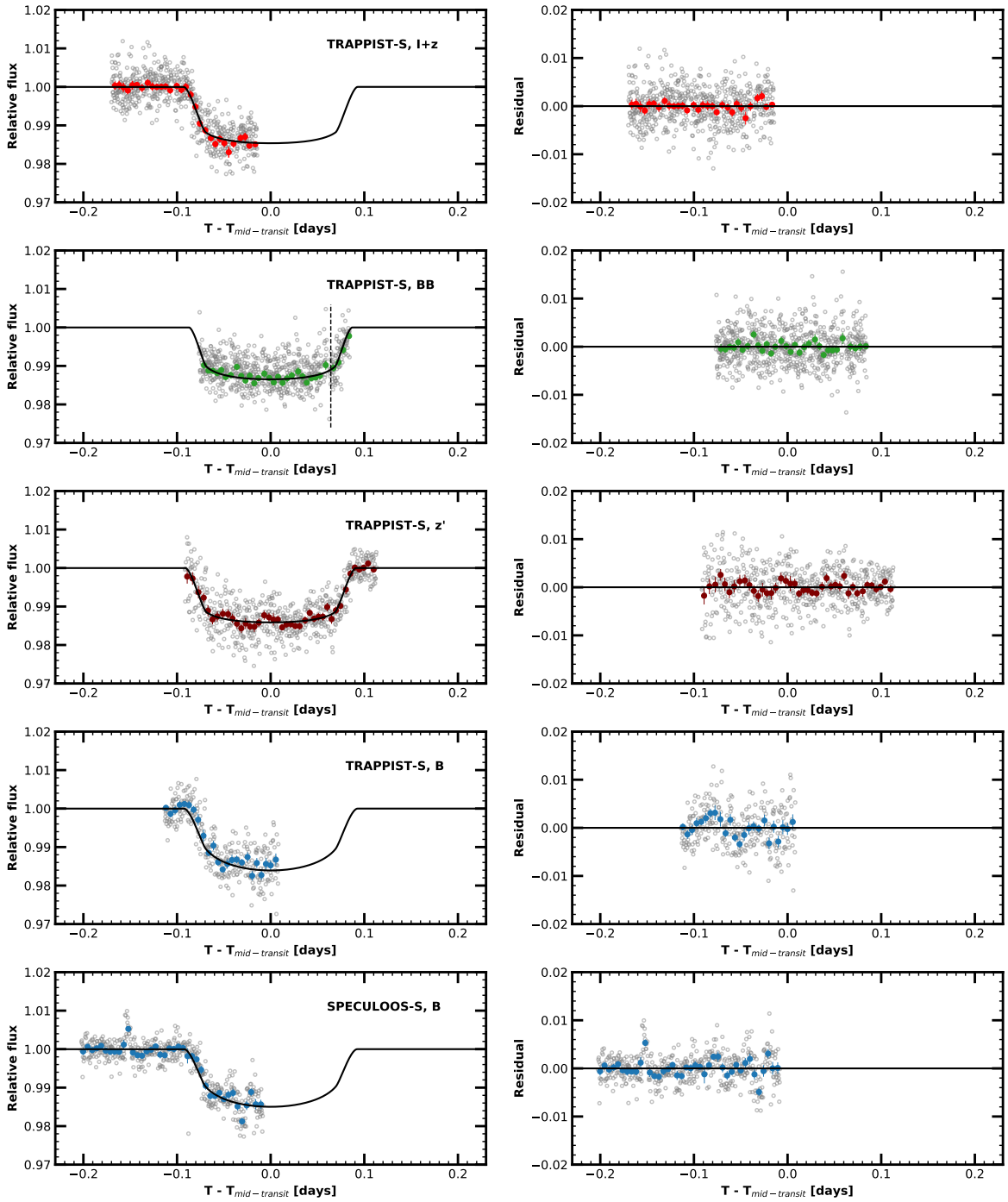

Figure 3: Follow-up transit photometry of WASP-193 b. *Left panels:* Four transits observed by TRAPPIST-South and one by SPECULOOS-South, period-folded using the best-fitting transit ephemeris deduced from our global MCMC analysis. Each individual transit light curve has been corrected by the baseline model presented in Table 5. The coloured points are data binned to 7.2 min and the best-fitting model is superimposed in red. *Right panels:* Residuals from the fits for each transit light curve.

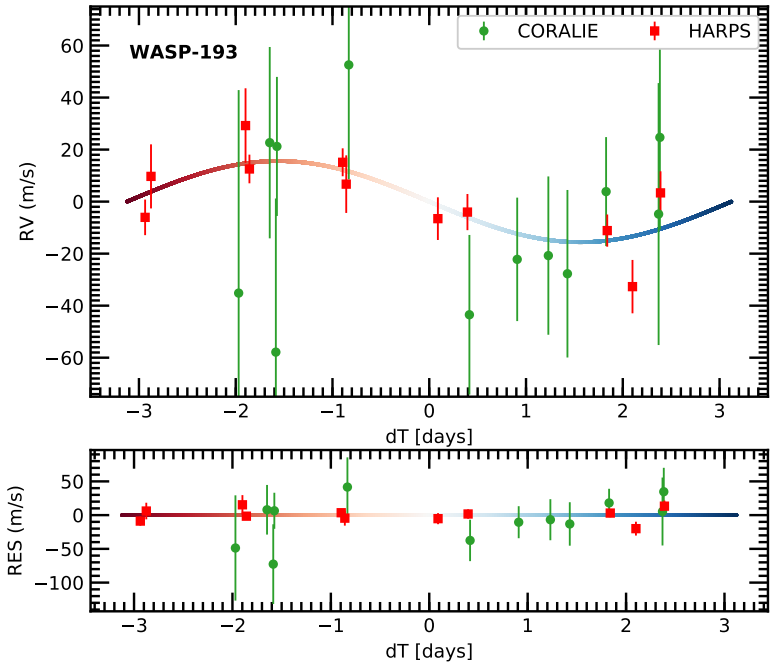

Figure 4: *Top panel:* RVs obtained with the CORALIE and HARPS spectrographs for WASP-193 period-folded using the best-fitting orbital model is superimposed as a solid line (in $m\ s^{-1}$). *Bottom panel:* RV residuals of the fit (in $m\ s^{-1}$). The green circles show the CORALIE data and the red squares show the HARPS data.

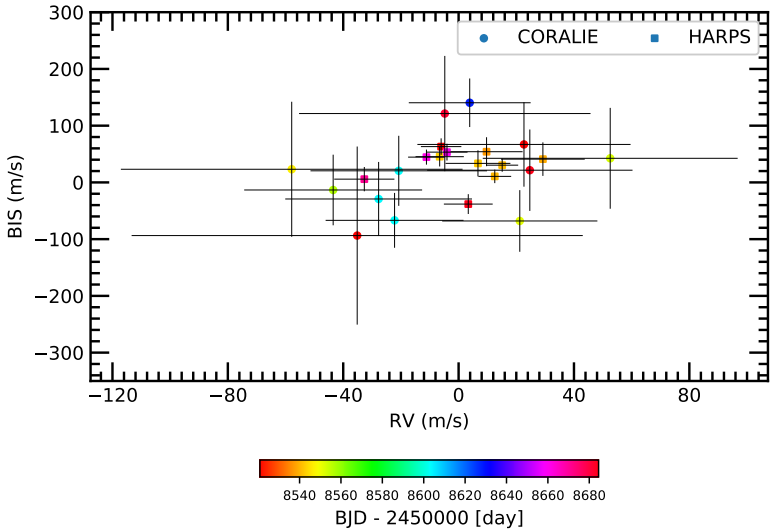

Figure 5: Bisector-span as a function of RV (in $m\ s^{-1}$) of WASP-193 obtained with the CORALIE and HARPS spectrographs. We assumed that the bisector-span error bars as twice the RV error bars. There is no significant correlation between the bisector-spans and RVs (the resulting p-value was found to be 0.124 ± 0.591 for HARPS and 0.705 ± 0.666 for CORALIE); therefore, in agreement with the planetary origin of the Doppler signal.

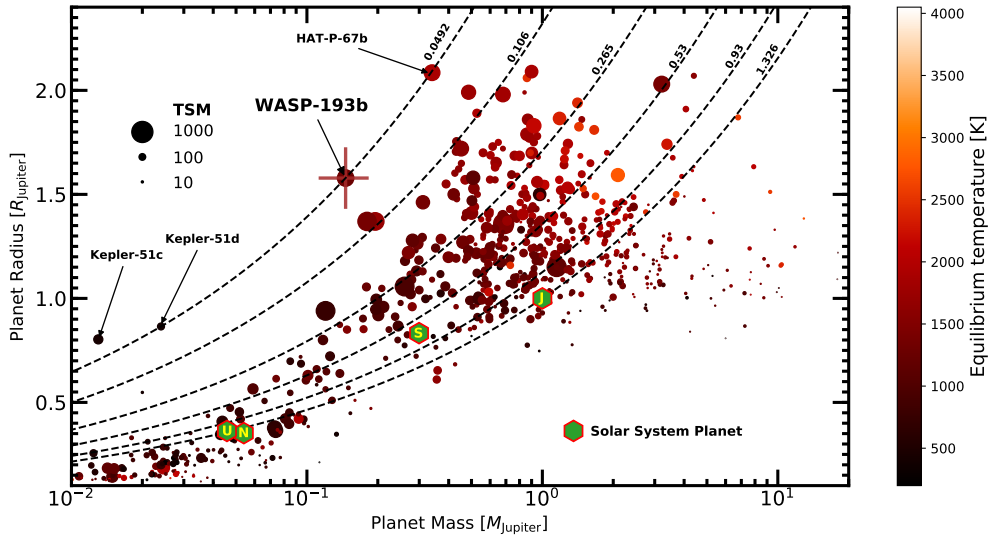

Figure 6: Mass–radius diagram of known transiting exoplanets from *NASA Archive of Exoplanets*. The size of the points scales with the Transmission Spectroscopy Metric (TSM[44]). The points are coloured according to their equilibrium temperature. The dashed black lines correspond to the different density curves of 0.049, 0.106, 0.265, 0.530, 0.930 and 1.326 g cm^{-3}, from left to right, respectively. WASP-193 b is shown with its corresponding error bars. The least dense planets known to date are labelled: Kepler-51 c, Kepler-51 d[46] and HAT-P-67 b[47]. Giant planets of the Solar System are shown as green points.

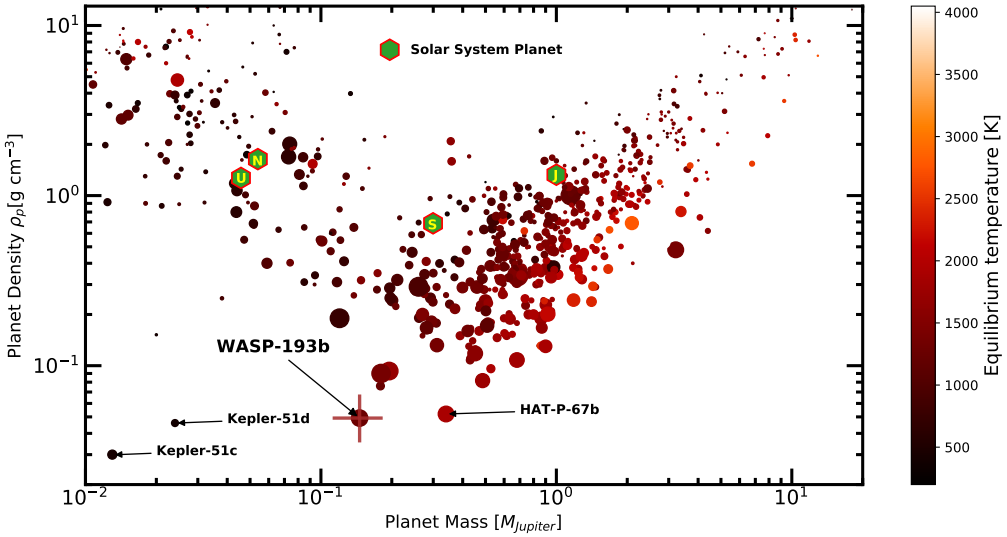

Figure 7: Mass–density diagram of known transiting exoplanets from *NASA Archive of Exoplanets*. The size of the points scales with the TSM[44]. The points are coloured according to their equilibrium temperature. WASP-193 b is displayed with its corresponding 1σ uncertainties. Giant planets of the Solar System are shown as green points. It is found that WASP-193 b is one of the lowest density planets discovered.

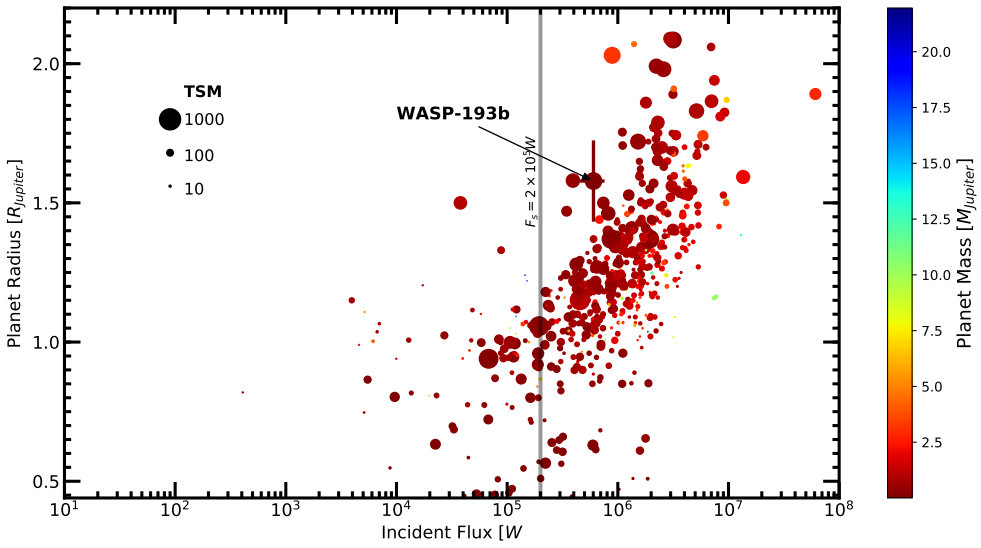

Figure 8: Planetary radii as a function of stellar incident flux of known transiting exoplanets from *NASA Archive of Exoplanets*. The size of the points scales with the TSM[44]. The points are coloured according to their mass. WASP-193 b is displayed with its corresponding 1σ uncertainties. The radii begin to show a correlation with stellar incident flux at $\sim 2 \times 10^5$ W m^{-2} (vertical gray line)[48].

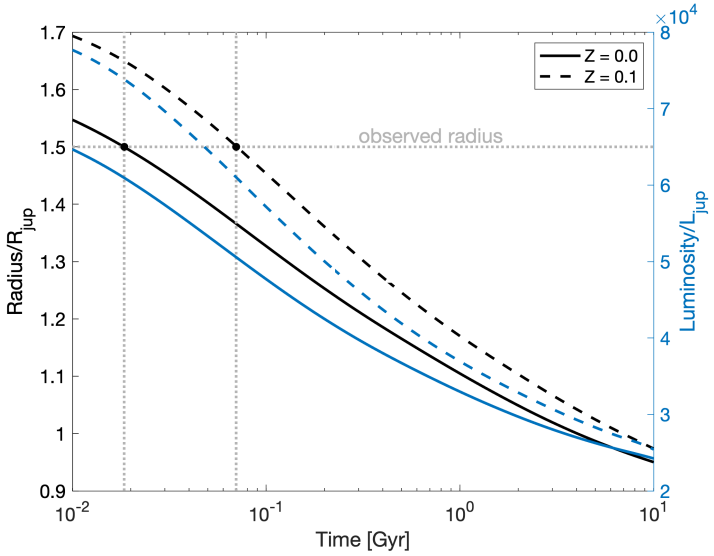

Figure 9: Radius (left axis) and luminosity (right axis) as a function of time. Two interior models with different metallicities (Z = 0, Z = 0.1) are shown. Grey dotted lines mark the observed radius of 1.5 R_{Jup}. The slow cooling of the model with a low metallicity of Z = 0.1 allows for larger radii compared to a pure H/He composition; only after more than 6 Gyrs, the radius for the pure H/He composition becomes larger than for the model with Z = 0.1.

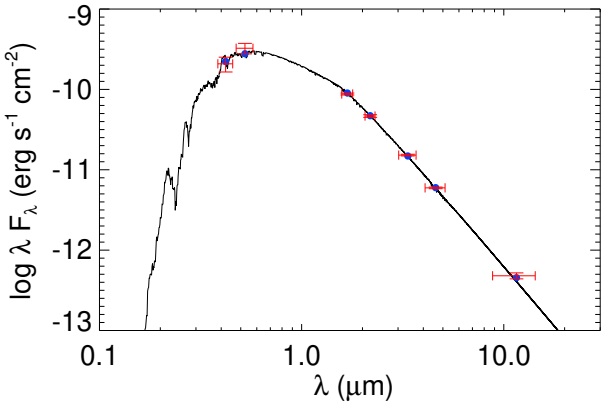

Figure 10: SED model (black line) of WASP-193 and the *EXOFASTv2* fit with broads and averages (blue circles) and broadband measurements (red). The error bars in wavelength denote the bandwidth of the corresponding filter and the error bars in flux denote the measurement uncertainties.

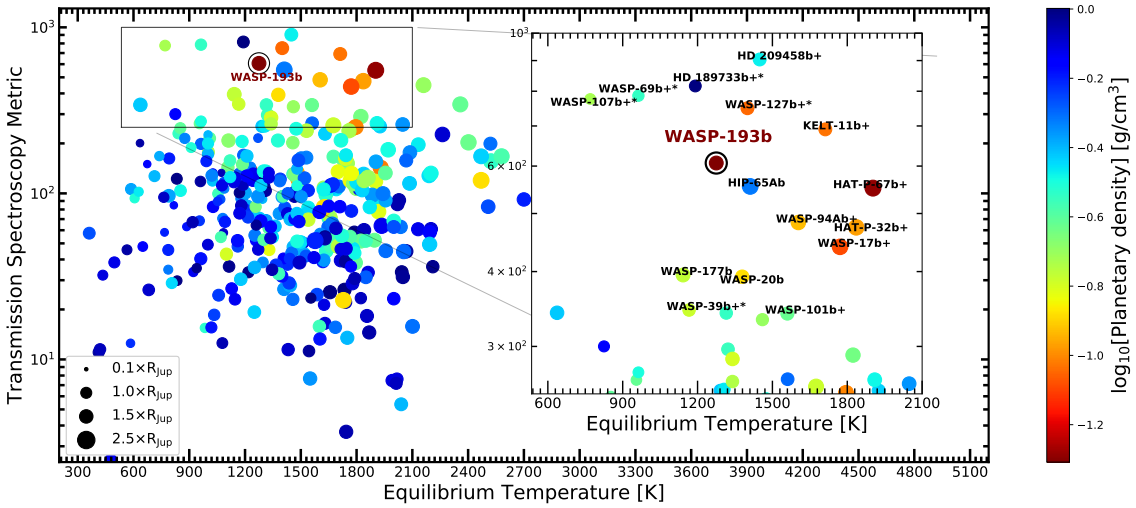

Figure 11: Feasibility of WASP-193 b for transmission spectroscopy studies. The transmission spectroscopy metric (TSM) is presented as a function of planetary equilibrium temperature of known transiting exoplanets from the *NASA Exoplanet Archive*. The point size scales with the planetary radius. The points are coloured according to their planetary density. WASP-193 b is highlighted by the black circle. Targets for which HST and/or JWST observations are scheduled/executed are shown by + and *, respectively.

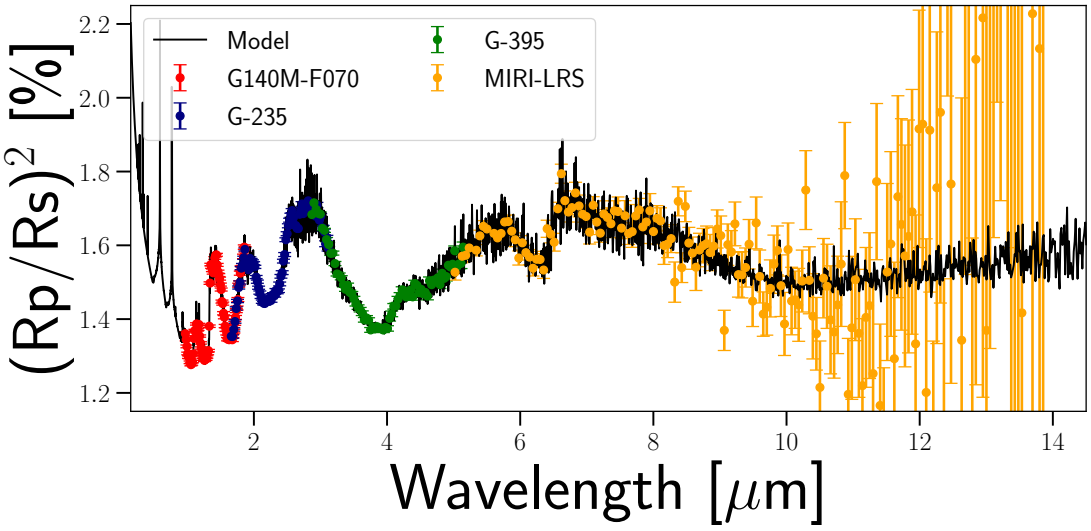

Figure 12: Synthetic transmission spectrum model of WASP-193 b in the *JWST* computed with petitRADTRANS pipeline[49] showing favorable detectability of multiple molecules using JWST single transit observation with G-140, G-235, G-395 and MIRI instruments.

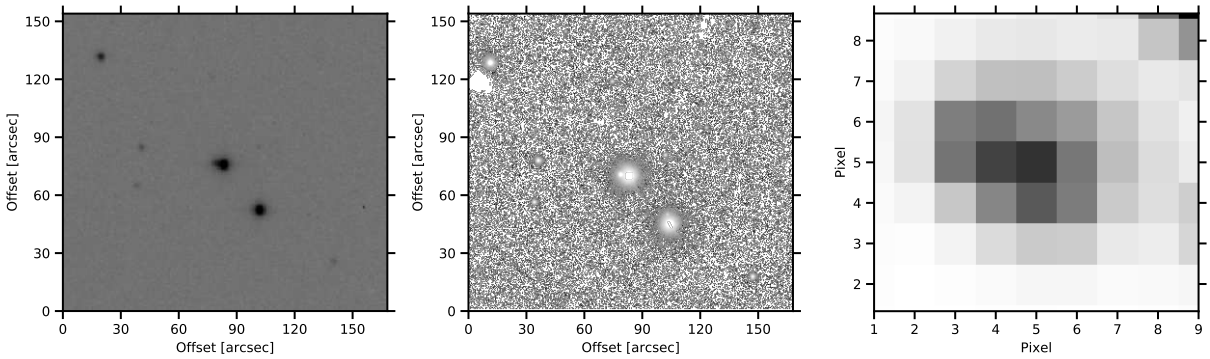

Figure 13: *Left panel:* TRAPPIST-South z' image cropped on a 150×150" region around WASP-193. *Middle panel:* Pan-STARRS[50] z' image of the same 150×150" region around WASP-193 with an image-scale of 0.25" pixel^{-1}. *Right panel: TESS* 150×150" image with the same FOV as left and middle panels.

Star informations		
Parameter	WASP-193	Source
Identifying informations:		
WASP_ID	1SWASPJ105723.88-295949.6	
GAIA_DR2_ID	5453063823882876032	Ref. [51]
2MASS_ID	10572385-2959497	Ref. [52]
RA [J2000]	$10^h57^m23.88^s$	
Dec [J2000]	$-29°59'49.6''$	
Parallax and distance:		
Plx [mas]	2.7336 $\pm$ 0.0402	Ref. [51]
Distance [pc]	365.82 $\pm$ 5.38	Ref. [51]
Photometric properties:		
V_{mag} [APASS]	12.189 $\pm$ 0.091	Ref. [53]
B_{mag} [APASS]	12.718 $\pm$ 0.032	Ref. [53]
J_{mag} [2MASS]	10.95	Ref. [52]
H_{mag} [2MASS]	10.810$\pm$ 0.034	Ref. [52]
K_{mag} [2MASS]	10.745 $\pm$ 0.035	Ref. [52]
G_{mag} [Gaia_DR2]	12.0421 $\pm$ 0.0003	Ref. [51]
$W1_{mag}$ [WISE]	10.64 $\pm$ 0.026	Ref. [54]
$W2_{mag}$ [WISE]	10.68 $\pm$ 0.026	Ref. [54]
$W3_{mag}$ [WISE]	10.491 $\pm$ 0.093	Ref. [54]
Stellar parameters from spectroscopic analysis		
$T_{\rm eff}$ [K]	6076 $\pm$ 120	Ref. [20]
$\log g_\star$ [dex]	4.256 $\pm$ 0.044	Ref. [20]
$[Fe/H]$ [dex]	-0.16 $\pm$ 0.09	Ref. [20]
$V \sin(i)$ [km/s]	4.3 $\pm$ 0.8	Ref. [20]
v_{macro} [km/s]	4.45	Ref. [55]
v_{micro} [km/s]	1.17	Ref. [55]
Spectral type	F9	Ref. [56]

Table 1 Astrometry, photometry and spectroscopy derived stellar properties of WASP-193.

Parameter	Value ± Error bar	Source
$T_{\rm eff}[K]$	$\mathbf{6076 \pm 120}$	HAPRS/CORALIE
	6040 ± 92	EXOFASTv2
$[Fe/H]$	$\mathbf{-0.16 \pm 0.09}$	HARPS/CORALIE
	-0.193 ± 0.086	EXOFASTv2
$\log g_\star$ [dex]	$\mathbf{4.256 \pm 0.044}$	HARPS/CORALIE
	4.289 ± 0.029	EXOFASTv2
$M_\star[M_\odot]$	1.15 ± 0.15	MCMC
	$0.975^{+0.064}_{-0.056}$	EXOFASTv2
	1.117 ± 0.061	BAGEMASS
$R_\star[R_\odot]$	$1.319^{+0.091}_{-0.096}$	MCMC
	$1.172^{+0.037}_{-0.034}$	EXOFASTv2
$L_\star[L_\odot]$	$2.11^{+0.38}_{-0.34}$	MCMC
	$1.65^{+0.13}_{-0.12}$	EXOFASTv2
Age [Gyr]	4.95 ± 1.34	BAGEMASS
	$7.6^{+2.7}_{-2.4}$	EXOFASTv2

Table 2 Parameters of the star WASP-193 derived from the analysis of the co-added HARPS and CORALIE spectra[20] and with the EXOFASTv2 pipeline[57]. The age of the star was inferred from a stellar evolution modeling with the BAGEMASS pipeline[58]. Stellar atmospheric parameters in bold are the adopted stellar priors used for our global analysis presented in Section 1.

Parameter	Symbol	Value	Unit
Jump parameters			
Planet/star area ratio	$(R_p/R_\star)^2$	1.448 ± 0.009	%
Impact parameter	$b' = a\cos i_p/R_\star$	$0.41^{+0.08}_{-0.14}$	$R_\star$
Transit duration	W	0.1828 ± 0.0026	days
Transit-timing	T_0	7781.66564 ± 0.00056	BJD - 2450000
Orbital period	P	6.2463345 ± 0.0000003	days
RV semi-amplitude	K	14.8 ± 3.1	m s^{-1}
Deduced stellar parameters	**WASP-193**		
Mean density	$\rho_\star$	$0.497^{+0.085}_{-0.061}$	$\rho_\odot$
Stellar mass	$M_\star$	1.15 ± 0.15	$M_\odot$
Stellar radius	$R_\star$	$1.319^{+0.091}_{-0.096}$	$R_\odot$
Luminosity	$L_\star$	$2.11^{+0.38}_{-0.34}$	$L_\odot$
Deduced planet parameters	**WASP-193 b**		
Scaled semi-major axis	$a/R_\star$	$11.30^{+0.61}_{-0.48}$	$R_\star$
Orbital semi-major axis	a	0.0695 ± 0.0031	au
Orbital inclination	i_p	$87.83^{+0.72}_{-0.50}$	deg
Eccentricity	e	0 (fixed)	
Density	ρ_p	$0.049^{+0.017}_{-0.013}$	g cm^{-3}
Surface gravity	$\log g_p$	$2.18^{+0.10}_{-0.11}$	cgs
Mass	M_p	0.146 ± 0.033	$M_{\rm Jup}$
Radius	R_p	1.58 ± 0.14	$R_{\rm Jup}$
Roche limit	a_R	$0.0360^{+0.0042}_{-0.0040}$	au
Equilibrium temperature	$T_{\rm eq}$	1275 ± 40	K
Irradiation	S_p	$6.024^{+0.765}_{-0.710} \times 10^5$	Wm^{-2}

Table 3: The WASP-193 system parameters derived from our global MCMC analysis (medians and 1σ limits of the marginalized posterior probability distributions).

LD coefficient	WASP-193
$u_{1,z'}$	0.207 ± 0.013
$u_{2,z'}$	0.288 ± 0.007
$u_{1,I+z}$	0.224 ± 0.014
$u_{2,I+z}$	0.291 ± 0.006
$u_{1,Johnson-B}$	0.543 ± 0.026
$u_{2,Johnson-B}$	0.209 ± 0.019
$u_{1,BB}$	0.276 ± 0.015
$u_{2,BB}$	0.298 ± 0.064
$u_{1,TESS}$	0.252 ± 0.015
$u_{2,TESS}$	0.295 ± 0.005

Table 4 Quadratic (LD) coefficients, u_1 and u_2, used in our MCMC analyses.

Observation parameters								MCMC analysis				
Target	Date	Telescope	Filter	N_p	$ExpT$ (s)	Duration (min)	$FWHM$ (pixel)	Baseline function	$\sigma_{7.2m}(\%)$	β_w	β_r	CF
WASP-193	02 Jan 2015	TRAPPIST-S	$I+z$	638	10	224	2.90	$f(t^1, f^1)$	0.0043	1.09	2.27	2.48
WASP-193	06 Apr 2015	TRAPPIST-S	BB	724	8	230	2.67	$f(a^1, O)$	0.0037	0.85	1.65	1.40
WASP-193	27 Jan 2017	TRAPPIST-S	z'	602	20	297	3.28	$f(t^1, b^1)$	0.0042	1.00	1.34	1.34
WASP-193	08 Jun 2019	TRAPPIST-S	B	292	25	176	3.32	$f(t^1, b^1)$	0.0042	0.74	1.60	1.18
WASP-193	08 Jun 2019	SPECULOOS	B	484	15	280	5.02	$f(t^1, a^1)$	0.0034	0.63	1.93	1.20

Table 5: The table shows the observational and MCMC analysis parameters. *Observation parameters*: date of observation, telescope, filter(s) used, number of images, exposure time(s), observation duration and FWHM of the point-spread function. *MCMC analysis parameters:* selected baseline-function, standard deviation (RMS) of the best-fitting residuals, deduced values of $\beta_{\rm white}$, $\beta_{\rm red}$ and the coefficient correction $CF = \beta_{\rm white} \times \beta_{red}$. For the baseline-function, $f(\varepsilon^n)$, denotes, respectively, the $n-$order polynomial function of the airmass ($\varepsilon = a$), FWHM ($\varepsilon = f$), background sky ($\varepsilon = b$), x & y positions ($\varepsilon = xy$), and the time ($\varepsilon = t$). The symbol O denotes an offset fixed at the time of the meridian flip.

JD - 2.450.000	RV [Km/s]	σ_{RV} [Km/s]	Instrument
7189.495005	-3.20480	0.03043	Euler-1.2m/CORALIE
7192.541007	-3.21921	0.07803	Euler-1.2m/CORALIE
7370.835932	-3.21178	0.03220	Euler-1.2m/CORALIE
7399.808035	-3.13149	0.04401	Euler-1.2m/CORALIE
7407.794853	-3.20625	0.02373	Euler-1.2m/CORALIE
7433.698835	-3.18020	0.02095	Euler-1.2m/CORALIE
7748.849031	-3.24191	0.05906	Euler-1.2m/CORALIE
7750.849267	-3.22754	0.03067	Euler-1.2m/CORALIE
7752.804569	-3.18884	0.05035	Euler-1.2m/CORALIE
7917.511102	-3.16284	0.02673	Euler-1.2m/CORALIE
8277.509694	-3.15936	0.03543	Euler-1.2m/CORALIE
8298.463390	-3.16139	0.03678	Euler-1.2m/CORALIE
8520.833792	-3.20823	0.01026	ESO-3.6m/HARPS
8537.867181	-3.17957	0.00695	ESO-3.6m/HARPS
8539.862413	-3.17219	0.00829	ESO-3.6m/HARPS
8540.782640	-3.18160	0.00684	ESO-3.6m/HARPS
8541.860510	-3.16300	0.00551	ESO-3.6m/HARPS
8542.824208	-3.16043	0.00537	ESO-3.6m/HARPS
8543.807974	-3.18210	0.00820	ESO-3.6m/HARPS
8660.500666	-3.14632	0.01434	ESO-3.6m/HARPS
8661.541276	-3.16883	0.01107	ESO-3.6m/HARPS
8670.484865	-3.18669	0.00619	ESO-3.6m/HARPS
8684.509150	-3.16585	0.01232	ESO-3.6m/HARPS

Table 6: Radial-velocities measurements for WASP-193 obtained from Euler-1.2m/CORALIE and ESO-3.6m/HARPS spectrographs.

1 Methods

WASP observations and data reduction

The Super-WASP project consists of data obtained at telescopes located at two sites: Sutherland Station of the South African Astronomical Observatory (SAAO) and the Observatorio del Roque de los Muchachos on the island of La Palma in the Canary Islands. The field-of-view (FOV) of each instrument is 482 deg^2 with a pixel scale of 13.7" pixel^{-1}. These instruments are capable of obtaining photometry with a precision better than 1% for objects with V-magnitudes between 7.0 and 11.5[1]. The hot-star WASP-193* was observed by the WASP-South survey in 2006 and 2014. The WASP-South data calibration (bias and dark subtraction, and flat-field division) was done with STARLINK pipeline[8] developed in Fortran. Aperture photometry was performed on the final calibrated images, where the stars fluxes were measured in three apertures with radii of 2.5, 3.5 and 4.5 pixels, following the method described by ref. [1,8,9].

TRAPPIST-South photometry

TRAPPIST (TRAnsiting Planets and PlanetesImals Small Telescope) network is composed of the 0.6-m twin robotic telescopes TRAPPIST-South and TRAPPIST-North[10,11,59]. For WASP-193, we used TRAPPIST-South located at the La Silla observatory in Chile. It is equipped with a thermo-electrically 2K×2K FLI ProLine PL3041-BB CCD camera with a FOV of 22'×22' and a pixel scale of 0.65". TRAPPIST-South observed a full transit of WASP-193 b in the Sloan-z' filter on 27 January 2017 with an exposure time of 20s, three partial transits, one in the $I + z$ filter on 02 January 2015 with an exposure time of 10s, one in the BB (blue-blocking) filter on 06 April 2015 with an exposure time of 8s, and a last one in the Johnson-B filter on 08 June 2019 with an exposure time of 25s. Data calibration and differential photometry were performed using the *PROSE*† pipeline[60]. The reduced light curves obtained of WASP-193 are presented in Fig. 3.

SPECULOOS-South photometry

The SPECULOOS (Search for habitable Planets EClipsing ULtra-cOOl Stars) robotic telescope network is composed of the SPECULOOS Southern Observatory (SSO), with four 1-m telescopes at ESO Paranal Observatory in Chile[12–14] and two 1-m telescopes in the Northern hemisphere: the SPECULOOS Northern Observatory (SNO) at Teide Observatory in Spain and SAINT-EX (Search And characterIsatioN of Transiting EXoplanets) at San Pedro Mártir Observatory in Mexico[61]. We observed a partial transit of WASP-193 b with one of the four telescopes of SSO on 08 June 2019 in the Johnson-B filter with an exposure time of 25s. Data calibration and differential photometry were performed using the *PROSE* pipeline[60]. The reduced light curve obtained is presented

*Other stellar designations: 1SWASPJ105723.88-295949.6 = TYC 6647-516-1 = DR2_id_5453063823882876032 = 2MASS_10572385-2959497

†*PROSE*: https://github.com/lgrcia/prose

in Fig. 3.

TESS photometry

The *TESS* (Transiting Exoplanet Survey Satellite[17]) mission was launched by NASA in April 2018. Its main goal is to detect and characterise transiting exoplanets smaller than Neptune orbiting nearby bright stars. *TESS*'s combined FOV is $24^\circ \times 96^\circ$, and one pixel is ~ 21" on the sky. WASP-193 was observed by *TESS* with the 30-min cadence in the ninth sector of its primary mission (from 28 February to 16 March 2019) and with 10-min cadence during its extended mission (from 07 March to 02 April 2021). We used the *TESScut* [‡] website to download the calibrated full-frame images (FFI). TESS's FFIs are widely used to search for transits on the stars that were not selected for the 2-min sampling[62,63]. The data calibration was done by the SPOC pipeline (*TESS* Science Processing Operations Center) as described by ref. [64]. Photometric reduction was then performed with the *Python/Photutils* package. The resulting light curve of WASP-193 is presented in Fig. 2.

Spectroscopic and radial-velocity measurements

In this paper, we used RV measurements obtained by CORALIE (mounted on the 1.2-m Swiss Euler telescope located at ESO La Silla in Chile[15]) and HARPS (mounted on the 3.6-m telescope at ESO La Silla in Chile[16]) spectrographs. We obtained 12 (between June 2015 and June 2018) and 11 (between February and July 2019) spectroscopic measurements of WASP-193 with the CORALIE and HARPS spectrographs, respectively. We applied the cross-correlation method[18] on the observed spectra of WASP-193 to extract the radial velocity measurements presented in Table 6.

The RV measurements of WASP-193 are in phase with the ephemerides from the WASP-South photometric data. When fixing the offset between CORALIE and HARPS to 2 m/s, the strongest signal in the generalised Lomb-Scargle periodogram[65] coincides with the transit period of 6.25 days, though the significance is bellow 10% FAP. The RV measurements obtained with CORALIE and HARPS are presented in Table 6, and the phase-folded RV curve of WASP-193 is presented in Fig. 4. The corresponding RV based on the fitting linear slope, enables us to discard the blended eclipsing binary (BEB) scenario and to keep the planetary companion.

We used co-added spectra obtained with the CORALIE and HARPS spectrographs to produce a single spectra with a signal-to-noise ratio (SNR) of 75, which allowed us to better constrain the stellar atmospheric parameters of WASP-193 using the method described by ref. [20]. The metallicity, $[Fe/H]$, was computed from the Fe lines, the effective temperature, $T_{\rm eff}$, was computed from the Hα line, the surface gravity, $\log g$, was estimated from the Mg Ib and Na ID lines and the rotational velocity, $V \sin(i)$, was measured by assuming a macroturbulence value of $\rm v_{macro} = 4.45$ km s^{-1}, which was extracted from the calibration formula[55], and a microtur-

[‡]*TESScut:* https://mast.stsci.edu/tesscut

bulence value of $v_{\rm micro} = 1.17$ km s^{-1}, which was extracted from the calibration formula[66]. With these values, it was found that WASP-193 is a Sun-like star with $T_{\rm eff} = 6076 \pm 120$ K, $\log g_\star = 4.256 \pm 0.044$ dex, $[Fe/H] = -0.16 \pm 0.09$ dex and $V \sin(i) = 4.3 \pm 0.8$ km s^{-1}. Using the *MKCLASS* [§] program[56], we got a spectral-type of F9 from the observed HARPS spectrum. This is consistent with that estimated from the stellar atmospheric parameters and $B - V$ color index.

Stellar parameters from the *ExoFASTv2* analysis

As an independent check of the derived stellar parameters for WASP-193, we performed an analysis using the exoplanet fitting suite, *EXOFASTv2* [57,67]. *EXOFASTv2* uses a differential evolution MCMC to globally and simultaneously model the star and planet. The built-in Gelman–Rubin statistic[68,69] is used to check the convergence of the chains. A full description of *EXOFASTv2* was given by ref. [57].

Within the fit, the host star's parameters are determined using the SEDs (see Fig. 10) constructed from our broadband photometry, MESA Isochrones and Stellar Tracks (MIST) stellar evolution models[70,71]. For the SED fits performed within *EXOFASTv2*, we used photometry from APASS DR9 BV[53], 2MASS HK[52], and ALL-WISE W1, W2 and W3 [54], which are presented in Table 1.

We applied Gaussian priors to the parameters $T_{\rm eff}$, $\log g_\star$, and $[Fe/H]$ using the obtained values from the spectroscopic analysis (Section 1). We also enforced Gaussian priors on the Gaia DR2 [51,72] parallax (adding 82 μas to the reported value and adding 33 μas in quadrature to the reported error, following the recommendation of ref. [73]). We adopted an upper limit on the extinction of $A_V = 0.20$ from ref. [74] using their web interface[¶]. The results of *EXOFASTv2* fit are presented in Table 2.

Stellar parameters using *BAGEMASS*

We used the *BAGEMASS* [‖] software to determine the age and mass of the hot-star following the MCMC technique described by ref. [58]. *BAGEMASS* is based on the *GARSTEC* stellar evolution code[75]. *GARSTEC* uses the *FreeEOS* equation of state given by ref. [76]. The *BAGEMASS* software calculates the posterior probability distributions of the stellar age and mass given the $T_{\rm eff}$, metallicity, $[Fe/H]$, luminosity, $L_\star$, and density, $\rho_\star$. We set the effective temperature to $T_{\rm eff} = 6076 \pm 120$ K and metallicity to $[Fe/H] = -0.16 \pm 0.09$ dex (from the spectroscopic analysis), and the luminosity to $L_\star/L_\odot = 2.11^{+0.38}_{-0.34}$ and the density to $\rho_\star/\rho_\odot = 0.497^{+0.085}_{-0.061}$ (from the transit light curves). The resulting stellar age was found to be 4.95 ± 1.34 Gyr, while the resulting mass was 1.117 ± 0.061 M$_\odot$, which are in good agreement with the ones resulting from our global MCMC analysis (see Table 3).

[§] *MKCLASS:* http://www.appstate.edu/~grayro/mkclass/
[¶] https://irsa.ipac.caltech.edu/applications/DUST/
[‖] *BAGEMASS:* https://sourceforge.net/projects/bagemass/

Modelling of the spectroscopic and photometric data

We combined the spectroscopic and photometric observations of WASP-193 to determine the physical parameters of the planetary system. The stellar atmospheric parameters, $T_{\rm eff}$ and $[Fe/H]$ from our spectroscopic analysis, were coupled with the stellar density, $\rho_\star$, determined from our transit light curves to infer the stellar radius, $R_\star$, mass, $M_\star$, luminosity, $L_\star$ and other physical parameters, by comparison with stellar evolution models, *EXOFASTv2* and *BAGEMASS* presented in previous Sections.

We used a Markov-chain Monte Carlo (MCMC) algorithm[21] to sample the posterior probability distributions of the system's parameters, from which we extracted the median values and their 1σ-uncertainties. All photometric measurements contain additional faint ($G_{\rm mag} \sim 16$) neighbour star at 4.2" (see Fig. 13). The resulting dilution was found to be $< 5\%$. We take into account this dilution in our golbal analysis.

We modelled the RV curves using a 2-body Keplerian model[23] shown in Table 6, and the transit light curves using the model of Mandel & Agol[22] multiplied by a baseline model to correct for several external effects related to time, full-width half-maximum (FWHM), airmass, position dx, dy and background (see Table 5). The baseline model for each transit light curve was selected based on minimizing of the Bayesian information criterion (BIC) [77] using the formula:

$$BIC = \chi^2 + k \log(N), \tag{1}$$

where k is the number of free parameters and N is the number of data points. The light curve observed on 06 April 2015 with TRAPPIST-South contains a meridian flip (i.e. a 180° rotation that the German equatorial mount has to undergo when the target star passes the local meridian) at BJD $= 2457119.619198$ (see details in Table 5), that we modeled as a flux offset in our MCMC analysis.

The jump parameters in our MCMC analysis (i.e. parameters randomly perturbed at each step of the MCMC) were:

- $T0$: the transit timing;
- W: the total duration of the transit (i.e. duration between ingress and egress);
- $dF = R_p^2/R_\star^2$: the transit depth, where R_p and $R_\star$ are the planetary and stellar radii, respectively;
- $b' = a\cos(i)/R_\star$: the impact parameter, where i is the orbital inclination and a is the orbital

semi-major axis;

- P: the orbital period;
- $K_2 = K\ P^{1/3}\sqrt{1-e^2}$, where K is the semi-amplitude of the RV and e is the orbital eccentricity; and
- $\sqrt{e}\cos(w)$ and $\sqrt{e}\sin(w)$, where w is the argument of periastron.

The stellar parameters $T_{\rm eff}$, $[Fe/H]$, and M_* were also jump parameters in our analysis. For $T_{\rm eff}$, $[Fe/H]$, and $\log g_\star$, we applied Gaussian priors based on the results of our spectroscopic analysis.

We assumed a quadratic limb-darkening (LD) law to take into account the impact of limb-darkening on our transit light curves. For each filter, the quadratic LD coefficients, u_1 and u_2, were interpolated from the tables of ref. [78] using the stellar effective temperature, T_{eff}, and metallicity, $[Fe/H]$, obtained from our spectroscopic analysis. For the non-standard $I+z$ and BB filters, we took the averages of the values for the standard filters Ic and Sloan-z' for the $I+z$ filter, and Ic and Johnson-R for the BB filter. The LD coefficient values of u_1 and u_2 for each filter are presented in Table 4.

Two MCMC analysis were performed: in the first we assumed a circular orbit and the second we assumed an eccentric orbit. Our results are compatible with a circular orbit based on a Bayes factor $BC = \exp(-\Delta BIC/2) = 1360$. The non-circular solution enabled us to estimate an orbital eccentricity of $e < 0.13$ at a 3σ significance.

For each transit light curve, a preliminary MCMC analysis composed of one Markov-chain of 100 000 steps was performed to estimate the correction factor (CF), to rescale the photometric errors; here, $CF = \beta_{\rm red} \times \beta_{\rm white}$, where $\beta_{\rm red}$ is the red noise and $\beta_{\rm white}$ is the white noise, as described by ref. [21]. For the RVs, a $jitter$ noise (i.e, the quadratic difference between the mean error of the measurements and the standard deviation of the best-fitting residuals) of 22.3 m s^{-1} for CORALIE and 4.1 m s^{-1} for HARPS was added quadratically to the RV error bars. Then, a global MCMC analysis was performed composed of five-chains of 100 000 steps. Convergence of each chain was checked using the statistical test presented by Gelman-Rubin [68]. The deduced parameters of the WASP-193 system are presented in Table 3. We used the stellar mass and radius values obtained from the spectral energy distribution (SED) analysis as a prior probability distribution in our global MCMC analysis. The obtained results are in good agreement with the MCMC results presented in Table 3.

Facility WASP-South, TRAPPIST-South, SPECULOOS-South, TESS, CORALIE, and HARPS

Softwares *Matplotlib*[79], *Numpy*[80], *Astropy*[81], *SciPy*[82], *Lightkurve*[83], *Prose*[60], *Wotan*[84], *Photutils*[85], *EXOFATSv2*[57], *petitRADTRANS*[49]